iScience

CellPress
OPEN ACCESS

Article

# Linking the microarchitecture of neurotransmitter systems to large-scale MEG resting state networks

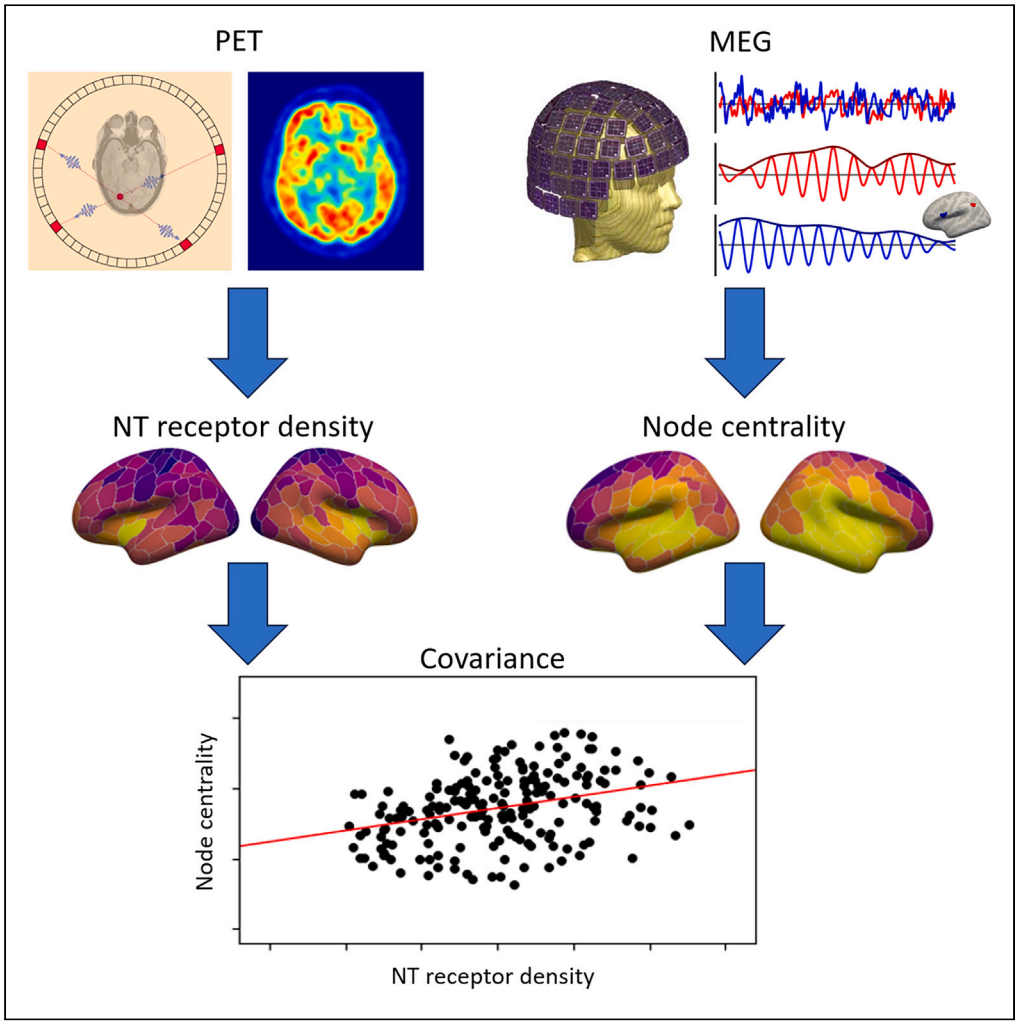


Felix Siebenhühner, J. Matias Palva, Satu Palva

satu.palva@helsinki.fi

## Highlights

Neurotransmitter receptor and transporter (NT-R/T) densities vary across the human cortex

Node centrality indexes hubness of brain regions in MEG phase and amplitude coupling networks

NT-R/T densities covary with node centrality in frequency- and region-specific patterns

Evidence that local receptor microarchitecture shapes macroscale networks

Siebenhühner et al., iScience *27*, 111111
November 15, 2024 
https://doi.org/10.1016/j.isci.2024.111111

iScience

CellPress
OPEN ACCESS

Article

# Linking the microarchitecture of neurotransmitter systems to large-scale MEG resting state networks

Felix Siebenhühner,[1,2,3,4] J. Matias Palva,[1,3,5] and Satu Palva[1,5,6,7,8,*]

## SUMMARY

**Neuronal oscillations are ubiquitous in brain activity at all scales and their synchronization dynamics are essential for information processing in neuronal systems. The underlying synaptic mechanisms, while mainly based on GABA- and glutamatergic neurotransmission, are influenced by neuromodulatory systems that have highly variable densities of neurotransmitter receptors and transporters across the cortical mantle. How they constrain the network structures of interacting oscillations has remained a central unaddressed question. We asked here whether the receptor and transporter densities covary with the frequency-specific neuroanatomical patterns of inter-areal phase synchrony (PS) and amplitude correlation (AC) networks in resting-state magnetoencephalography (MEG) data. Network centrality in delta and gamma frequencies covaried positively with GABA-, NMDA-, dopaminergic-, and most serotonergic receptor and transporter densities while covariance was negative in alpha and beta bands. These results show that local receptor microarchitecture shapes macro-scale oscillation networks in spectrally specific patterns.**

## INTRODUCTION

Collective neuronal activity is organized by rhythmic excitability fluctuations—neuronal oscillations—that characterize signals in the meso- and macroscopic population measurements from intra-cerebral local field potentials (LFP) in animal models and human stereo-electroencephalography (SEEG) to scalp electro- and magnetoencephalography (EEG/MEG) in humans, respectively.[1,2] Oscillations emerge across a wide range of frequencies and their spectrally and anatomically specific coupling provides a temporal clocking mechanism for dynamic routing of neuronal processing via oscillatory ensemble codes, which is thought to be fundamental for various behaviors and higher cognitive functions.[2–10] At the network level, frequency-specific hubs, i.e., brain areas serving as highly central nodes in the networks, are particularly crucial for information routing.[11–16]

Both a large body of neurophysiological evidence and computational biophysical models of neuronal circuit mechanisms suggest that synaptic interactions among excitatory pyramidal neurons (PNs) and GABAergic inhibitory interneurons (INs) form the simplest universal microcircuit that can intrinsically generate synchronized oscillations through recurrent and reciprocal interactions.[17–19] The oscillation frequency is determined by several factors including the strength of the excitatory drive, axonal conduction delays, and the time constants of $GABA_A$- and $GABA_B$-receptor mediated inhibitory post-synaptic potentials.[20] As is relevant for the present study, the PN-IN circuitry also receives efferent connections from neuromodulatory systems that impose heterogeneous influences.[21–25] Oscillations and their inter-areal interactions are thus dependent on the momentary local availability of various neurotransmitters (NTs) which are regulated by the local density of NT receptors and transporters among other mechanisms.[26–28]

The distinctive cortical projection patterns of neuromodulatory systems are paralleled by highly variable densities of neurotransmitter receptors and transporters across the cortical mantle.[29–33] Yet, the question how the local microarchitectural variability in NT receptor and transporter densities influences and constrains inter-areal coupling of neuronal oscillations has largely remained unanswered. Recently, datasets of various NT receptor and transporter densities in the human cortex obtained with position emission tomography (PET) data were collated by Hansen et al.[31] and mapped to different resolutions of the commonly used Schaefer atlas.[34] Based on this dataset and the *neuromaps*

[1]Neuroscience Center, Helsinki Institute of Life Science, University of Helsinki, Helsinki, Finland
[2]BioMag Laboratory, HUS Medical Imaging Centre, Helsinki University, Helsinki, Finland
[3]Department of Neuroscience and Bioengineering (NBE), Aalto University, Espoo, Finland
[4]Department of Electrical Engineering and Information Technology, Technical University Darmstadt, Darmstadt, Germany
[5]Centre for Cognitive Neuroimaging (CCNi), School of Psychology and Neuroscience, University of Glasgow, Glasgow, UK
[6]Division of Psychology, VISE, Faculty of Education and Psychology, University of Oulu, Oulu, Finland
[7]Senior author
[8]Lead contact
*Correspondence: satu.palva@helsinki.fi
https://doi.org/10.1016/j.isci.2024.111111

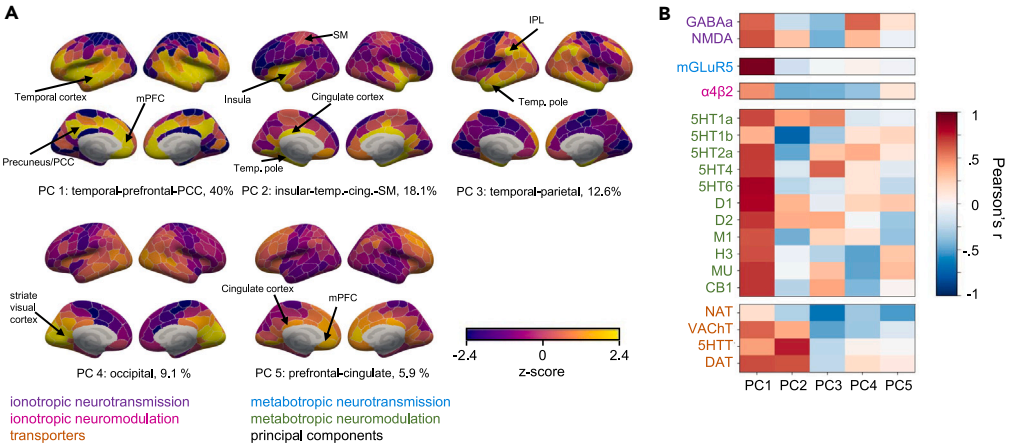


**Figure 1. Principal component analysis reveals common spatial patterns in the distribution of neurotransmitter receptors and transporters**

(A) The first five principal components (PCs) of the receptor and transporter density maps, with percentage of variance explained.

(B) PC loadings of individual density maps indicate shared neuroarchitectonical principles underlying the distribution of NT receptors and transporters in the human cortex. Loadings are quantified by Pearson's r between the PCs and individual density maps. See Figure S1 for the individual density maps.

toolbox,[35] several studies have explored how local neurotransmitter architecture is related to the local signal power in MEG data,[31,33] altered in disease,[36–39] and related to region-specific effects of pharmacological agents.[40]

Here, we set out to investigate the role that NT availability and neuromodulatory systems have in shaping the large-scale coupling of neuronal oscillations. We hypothesized that the emergent neuroanatomical structure of phase synchrony (PS) and amplitude correlation (AC) networks would co-vary with NT receptor and transporter densities. To test this hypothesis, we analyzed source-reconstructed human MEG data and assessed how node centrality, indexing the 'hubness' of individual brain regions, in large-scale PS and AC networks covaries with neurotransmitter receptor and transporter densities. We identified 6 frequency bands of interest in a data-driven manner and computed the covariance of node centrality (assessed with three different metrics) of these frequency bands and individual frequencies in the range 1–96 Hz with receptor and transporter densities. We further identified five leading principal components common to these density maps and assessed their covariance with node centrality as well. We found frequency- and coupling-mode-specific patterns of covariance between node centrality and receptor and transporter densities, showing that local microarchitecture indeed influences large-scale connectivity networks of neuronal oscillations in the human brain.

## RESULTS

### Principal component analysis reveals neuroarchitectonical principles underlying density maps of neurotransmitter receptors and transporters

We used the neurotransmitter receptor and transporter density maps[31] at the resolution of 200 cortical parcels in the Schaefer atlas[34] (Figure S1). Since many of these maps exhibited similar spatial patterns, we first identified the shared underlying patterns with principal component analysis (PCA). The first 5 components together explained 86.7% of variance in the density maps (40%, 18.1%, 12.6%, 9.1%, and 5.9%, respectively) and were used for subsequent analysis (Figure 1A). The further components each explained less than 5% variance and were therefore excluded from further analysis. We then estimated the "loading" of the individual density maps to these PCs with Pearson's correlation coefficient. Reproducing earlier findings,[31] the first component (PC1) was the strongest along the lateral sulcus around the insular and in medial prefrontal regions as well as in the precuneus and posterior cingulate cortex (PCC) (see Figure 1A) and was positively loaded for all density maps (Figure 1B). Thus, PC1 represents an overarching cortical architecture of receptor and transporter distributions.[41] In addition, we identified four more anatomically distinct principal components (PCs 2–5, see Figure 1). PC2 was most pronounced around the insula (similarly to PC1), but also included the medial temporal and cingulate cortex and was the only PC with positive loading in the somatomotor cortex. This component showed highest loadings with 5HTT, DAT, $D_1$, $D_2$, and glutamatergic NMDA and VAChT receptors and transporters. PC3, in contrast, was localized to the lateral temporal and intraparietal cortex, and had strongest loadings for $5HT_{1a}$, $5HT_{2a}$, $5HT_4$, $D_2$, MU, CB1, and M1. PC4 was largest in visual regions, and had strong loadings for serotonergic, dopaminergic, GABA, and NMDA receptors and transporters. Finally, PC5 was the most salient in prefrontal and cingulate regions and had the strongest loadings for histamine, α4β2, MU, $5HT_{1b}$, and $D_1$ receptors.

### Phase synchrony and amplitude correlation networks are anatomically and spectrally specific

We performed source-reconstruction on 10-min resting-state MEG datasets from 67 healthy subjects (see STAR Methods and Table S1 for demographics) and collapsed source time series to the 200-parcel Schaefer atlas.[15] We quantified pairwise PS between parcel time series with the imaginary part of the complex phase locking value (iPLV)[42] and ACs with the orthogonalized correlation coefficient (oCC),[43,44] as

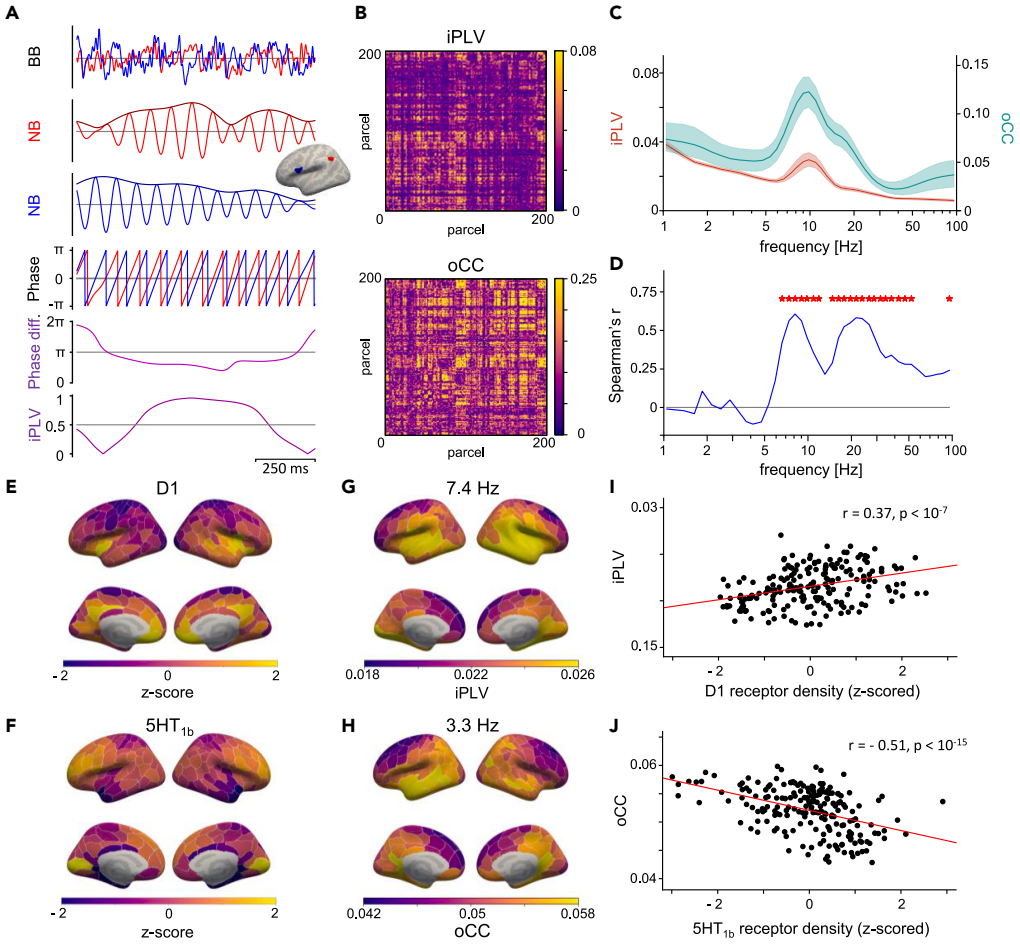


**Figure 2. Inter-areal phase synchrony and amplitude correlations**

(A) Example broadband (BB) time series from two cortical parcels (top), with their narrowband-filtered (NB, 10 Hz) real and amplitude time series (2nd, 3rd row) and phase time series (4th row) and the phase difference (5th row) and iPLV (bottom).

(B) Example amplitude correlation and phase synchrony interaction matrices, estimated with oCC and iPLV, resp., between all parcel pairs.

(C) Mean connectivity strength (across all 67 subjects) per frequency for oCC and iPLV, with 95% confidence intervals.

(D) Spearman's correlation between oCC and iPLV node strength across parcels. Significant correlations are marked with stars ($p < 0.05$, corrected with Benjamini-Hochberg).

(E) D1 receptor density per cortical parcel (z-scored).

(F) Same for 5HT1b receptor density.

(G) iPLV node strength per parcel at 7.4 Hz.

(H) oCC node strength per parcel at 3.3 Hz.

(I) Spearman's correlation across parcels between D1 receptor density and iPLV node strength at 7.4 Hz.

(J) Spearman's correlation across parcels between $5HT_{1b}$ receptor density and oCC node strength at 3.3 Hz. See Figure S2 for derivation of frequency bands and S3 for node strength in these frequency bands.

these metrics are insensitive to the direct effects of source leakage, i.e., will not yield false positives[2,42] (Figures 2A and 2B). In line with previous studies,[15,43–45] the mean strength of PS and AC connections exhibited an alpha band peak around 10 Hz while significant phase and ACs were observable throughout the studied frequency range from theta to gamma bands (Figure 2C). We next used a data-driven approach to identify clusters of frequencies that exhibited similar anatomical profiles of inter-areal connectivity patterns[46] in both PS and AC and then derived shared consensus frequency bands (Figure S2) for subsequent analyses: δ (1–3.5 Hz), low-θ (3.5–5.8 Hz), θ–α (5.8–9.5 Hz), high-α (9.5–15 Hz), β (15–32 Hz), and γ (32–96 Hz). We estimated in each frequency band the node strength as the mean iPLV or oCC strength of any given parcel with all other parcels (Figures S3A and S3B). Node strength was positively correlated between PS and AC (Figure 2D) in most frequencies from 5 Hz to 50 Hz, but most strongly in θ–α and β bands. To localize these differences, we obtained the z-scored maps of node strength and computed the difference PS - AC in each band (Figure S3C). The largest differences were observed around the occipital pole, which showed strong PS in all frequency bands except in β band, but strong AC only in θ to α bands. Other posterior regions showed stronger AC than PS in most frequency bands, while regions near the temporal pole and lateral sulcus showed higher PS in θ to α bands, but

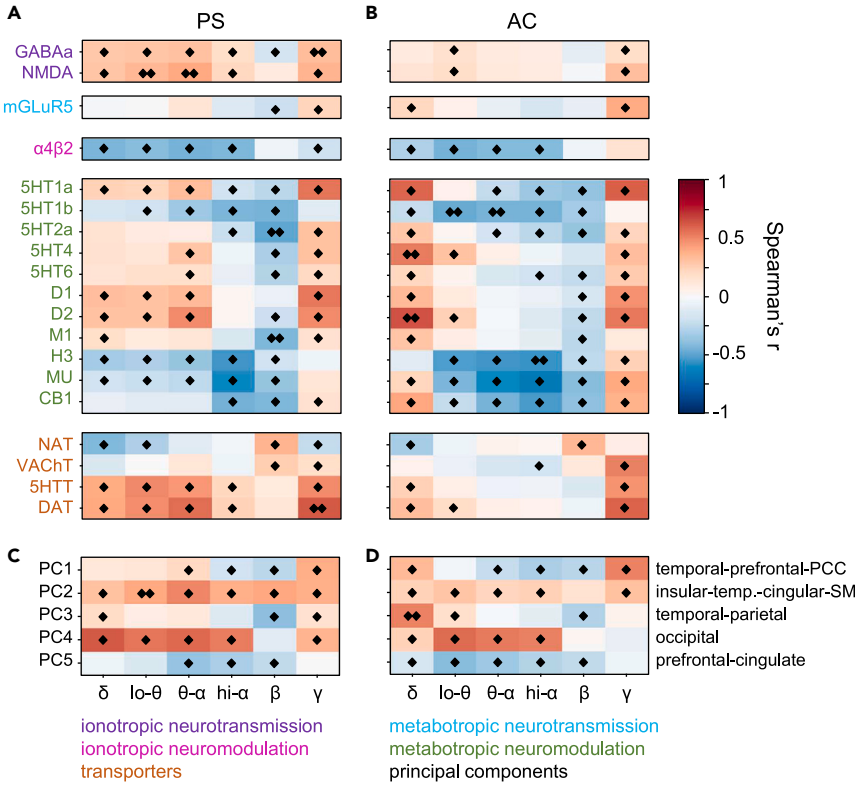


**Figure 3. Covariance of receptor and transporter density and node centrality varies with frequency band and coupling mode**

(A) Covariance of neurotransmitter receptor and transporter density with node centrality (node strength) in phase synchrony networks (averaged within frequency bands and across all 67 subjects) across all cortical parcels (Spearman's r); statistics were obtained from comparison with randomly permutated null models and with 'spin' null models preserving spatial autocorrelations ($N$ = 10,000; ◆: $p_{perm} < 0.05$; ◆◆: $p_{perm} < 0.05$ & $p_{spin} < 0.05$; all results with false-discovery reduction).

(B) Same as A, for node centrality in networks of amplitude correlations.

(C and D) Covariance between principal components and node centrality for PS and AC networks, respectively. See Figure S4 for covariance in Morlet frequencies, S5 & S6 for covariance with other metrics of node centrality, and S7 for covariance in males and females.

higher AC in δ and γ bands. These results provide further evidence for the hypothesis that AC and PS are related but constitute distinct coupling and communication mechanisms in cortical networks.[45,47,48]

## Frequency-band specific covariance of node centrality with receptor and transporter densities

We then set out to investigate the covariance of the node centrality in PS and AC networks with receptor and transporter densities. Node centrality is generally seen as an indicator of 'hub-ness', i.e., a measure of which nodes in a network are most central and important for information routing.[49] We here used node strength as our primary metric of node centrality, but also utilized node degree and betweenness centrality as alternative centrality metrics.[49,50] We computed Spearman's correlation coefficient between node centrality and each receptor's or transporter's density across parcels (Figures 2E–2J), both for the identified frequency bands (Figure 3) and single frequencies (Figure S4). Significance of covariances was assessed against correlation coefficients from both random permutations ($N_{perm}$ = 10,000) as well as against 'spin' permutations ($N_{spin}$ = 10,000) that preserve the spatial autocorrelations in MEG data and therefore are considerably more conservative[31,51] (exact r and *p*-values are provided in Tables S2 and S3). For both of these tests, we performed false discovery reduction by eliminating the expected fraction of false positives.[15,46]

We first assessed the covariance of neuronal oscillations with $GABA_A$ and NMDA receptor densities, which through fast ionotropic neurotransmission underlie the generation of oscillations in local circuits of interacting glutamatergic excitatory pyramidal or principal neurons (PNs) and inhibitory GABAergic interneurons (INs).[21,22,52–55] Both $GABA_A$ and glutamatergic NMDA receptor densities covaried positively with PS node strength in δ−α and γ frequency bands, such that most of these correlations were preserved also with conservative spin permutation statistics, while covariance with AC occurred only in low-θ and γ bands (Figures 3A, 3B, and S4). These findings are thus in line with biophysical models of generation of oscillatory synchronization in PN-IN circuitry across a wide frequency range. Results obtained for both node degree and betweenness centrality in sparse networks of 50% and 20% edge density (Figures S5 and S6) were largely similar, which underscored the robustness of the observed relationships. This result provides further evidence for the importance of $GABA_A$ and NMDA receptors in the generation of long-range phase-synchronization as well as for AC and PS resulting from the distinct circuit mechanisms.

The densities for the metabotropic excitatory receptor mGluR5 (metabotropic glutamate receptor 5) as well as receptor and transporter densities receptor of the main neuromodulatory NTs – DA, 5HT (except $5HT_{1b}$), and ACh – also covaried with node centrality in partially distinct patterns. Covariance was positive for both PS and AC in δ and γ bands, and for PS also in θ–low-α bands. The most robust correlations were found for δ band AC node strength with $5HT_4$ and $D_2$ receptor densities, for γ band PS node strength with $D_1$ receptor density with, and dopamine transporter (DAT) density with γ band node strength in both PS and AC. For the in-between frequency bands (hi-α and β band PS and θ−β band AC), covariance of node centrality with receptor densities was zero or negative, indicating that peripheral rather than central nodes in these networks corresponded to high receptor density. Negative covariances of $5HT_{2a}$ and M1 with PS and $5HT_{1b}$ and $H_3$ with AC were preserved also with spin permutation statistics, indicating high spatial specificity of these negative covariance patterns.

These results demonstrate a differential influence of neuromodulatory NTs on oscillatory coupling in δ and γ bands vs. α and β bands. This finding is intriguing given the differential roles of these frequency bands to information processing in neuronal circuits and may provide a putative explanation for the differences across these frequencies in mediating cortical computations.[5,56,57]

The relative differences between AC and PS are in line with the suggestions of AC reflecting slower non-synaptic connectivity[48,58,59] and PS and AC being related but dissociable mechanisms supporting at least partially different computational functions.[45,47] The covariance of low-α and high-α band node centrality with receptor densities for PS but not for AC networks is intriguing as alpha-band PS is associated with top-down control[12,56,60] while alpha-amplitudes are associated with decreased excitability and inhibition of neuronal processing.[61–63] Notably, also the densities of nicotine acetylcholine receptor (α4β2) and of the metabolic and hormonic receptors MU (mu-opioid), $H_3$ (histaminergic), $CB_1$ (cannabinoid) covaried with node centrality negatively for PS, but positively for AC in γ and partially also in δ band. These findings suggest that differences between PS and AC networks, as well as those across different frequency bands, arise due to their generation in different cytoarchitectonic circuits.

In order to test for effects specific to biological sex, we repeated the covariance analysis separately for males ($N$ = 35) and females ($N$ = 32) and found that the larger covariance patterns were similar in both sexes with only small variations (Figure S7).

### Principal components reveal shared covariance patterns of receptor density with node centrality

We then computed the covariance of the PCs with node centrality. The temporal-prefrontal-PCC component PC1 – which had positive loadings for all receptors – showed positive covariance with θ-α and γ PS and δ and γ AC node strengths (Figures 3C and 3D) and negative covariances for most in-between frequencies. This covariance pattern was reminiscent of those for 5HT and DA receptors and transporters and mGluR5 which had the strongest loading on this PC. Similar covariances were observed also for node degree and betweenness centrality (Figures S5 and S6). In contrast, PC2 which had highest loadings for transporter densities and strongest expression in insular, temporal, cingulate, and somatomotor regions showed positive covariance across all frequency bands with PS and AC node centrality. The covariance of θ−α node centrality with PC2 was significant against spin permutations in low-θ and large in θ−α, strongly suggesting that NT clearance by transporters may be critical specifically for θ−α band oscillations that are abundantly present during RS activity in the human cortex.

The temporal-parietal PC3 showed robust positive covariation with node centrality in δ band PS and AC networks, the correlations for AC being significant against spin permutations. As PC1 represented the expression of receptors and transporters in frontal-temporal and medial regions, and PC3 reflected their expression in temporal-occipital regions, these two may thus be seen as complementary architectures of dopaminergic, serotonergic, and glutaminergic neuromodulatory influence on inter-areal connectivity respectively. Similarly to PC2, PC4 showed strong covariance with PS node centrality in all frequency bands except for β band, and with AC node centrality in δ to α bands. As PC4 had highest loadings for $GABA_A$, dopaminergic, glutamatergic, and most serotonergic receptors, this is in line with well-known contributions of activity at these receptors to the generation of low frequency oscillations and phase synchronization in the visual cortex.[64]

In contrast to the other PCs, the prefrontal-cingulate PC5 with strongest loadings with $5HT_{1b}$, $H_3$, α4β2, MU, and $CB_1$ showed negative covariance with node centrality in line with similar covariance patterns for individual receptor densities. Overall, our results demonstrate that principal components of neurotransmitter system architecture influence oscillation-based connectivity networks in frequency- and anatomy-specific patterns.

## DISCUSSION

Flexibility of behavior and cognition is dependent on the diversity of neuromodulators and their receptors in neuromodulatory ascending systems and, in parallel, the flexible routing of information via phase- and amplitude-coupled neuronal oscillations. In this study, we demonstrate the covariance of neurotransmitter receptor and transporter density with MEG-derived phase- and amplitude-based connectivity of neuronal oscillations. These findings shed light on the multi-level structures and dynamics in the brain giving rise to connectivity, i.e., the human dynome.[65]

The present findings strongly suggest that cortical microarchitecture and macroscopic neuromodulator system projection patterns shape the coupling of neuronal network oscillations in frequency- and anatomy-specific patterns. These data thus yield experimental evidence from the human brain that the heterogeneity in receptor and transporter densities influences PS and ACs networks in different ways depending on the coupling mode and frequency which are indicative of different neurophysiological circuit mechanism underlying the emergence of these oscillations. First, these results are in agreement with neurophysiological data and biophysical models which have proposed that oscillations in theta, alpha, and gamma bands may arise from differential interactions between PNs and INs.[17,25,39] Second, our results add on to the cumulating evidence that PS and AC do not operationalize a shared unitary underlying construct, but rather reflect distinctive and complementary processes arising from different micro- and cytoarchitectonic structures, likely through distinct biophysical mechanisms. In PS,

pre-synaptic potentials from oscillation assembly will arrive during a time when they can have the maximal impact on a post-synaptic neuron which results in predictable windows for integration for an upstream reader[18] while AC might reflect slower coupling of local synchronization dynamics[48,58,59], supporting at least partially different computational functions.[45,47] Future studies, however, are needed to improve the mechanistic understanding of PS and AC in the context of synaptic mechanisms and biophysical models.

Previous studies have established that individual structural connectivity influences functional connectivity both in fMRI[66,67] and MEG.[32,60,68] Spectral and spatial heterogeneity in the correlation of brain structure and network dynamics is also predicted by whole-brain computational modeling approaches.[32,68,69] Our results advanced in this study establish that MEG derived oscillation-based networks are also dependent on the various neurotransmitters receptor and transporter densities. As neurotransmitter receptors and transporters are associated with regulation of synaptic neurotransmitter levels,[29,31–33] this suggests that coupling of neuronal oscillations is influenced by the instantaneous synaptic availability of the neurotransmitters in accordance with the biophysical models. Such heterogeneity of neurotransmitter receptor and transporter densities could also underlie the variability in the exhibition/inhibition (E/I) balance[24,46,70,71] and thereby also that of critical dynamics of phase synchronization.[69]

Critically, understanding how NT receptor and transporter density distributions influence neuronal processing is essential for understanding the mechanisms of brain disorders. Abnormal oscillations and abnormal NT function characterize a wide range of brain disorders[37–39,72] including schizophrenia,[73] depression,[41,74–76] Parkinson's disease[36] and ADHD.[77–80] Resolving the biological constraints on how oscillations are generated and modulated by neurotransmitters in a frequency- and region-specific manner[21,22] may improve our understanding of how neuromodulatory systems are affected by pharmacological agents[40] and contribute to a holistic and synergetic approach to understand brain disorders.[81]

Resolving how the brain's microanatomy influences oscillatory dynamics is fundamental for understanding information processing in neuronal networks. Here, we studied the covariance of node centrality of MEG-derived frequency-specific connectivity with neurotransmitter receptor and transporter density distributions. Our findings demonstrate that networks of oscillatory connectivity are influenced by organizational principles of the underlying distribution of neurotransmitter receptors and transporters impacting connectivity in a frequency-, region-, and coupling-mode-specific manner.

### Limitations of the study

Assessing significance in neuroimaging data is a complex issue. We here assessed the significance of observations using both the commonly adopted random permutations of the parcel order and the more conservative 'spin' permutations that preserve and, hence, also correct for spatial autocorrelations in PET and MEG data[31,51], as we believe that true covariance lies in between the two. Traditional permutation approaches underestimate the statistical inflation driven by spatial autocorrelations in neuroimaging data. Spin permutations, on the other hand, assume that the spatial autocorrelations are inherently a form of leakage in neuroimaging data. Neuromodulatory ascending systems, however, have intrinsically diffuse connectivity[24,71] and the spatial patterns in both MEG and fMRI neuroimaging data are closely related to spatial patterns in brain anatomy and geometry,[82–84] suggesting that a considerable fraction of spatial autocorrelations in MEG data may be driven by true short- and medium-range correlations in cortical activity rather than reflecting signal leakage exclusively.[85,86] Future studies are needed to investigate how connectivity patterns are influenced by the underlying neurotransmitter receptor and transporter densities not only in resting state, but also during tasks that selectively activates specific neuromodulatory systems.[87–89] Further insights might also be gained if density maps would become available and related to connectivity for other important receptors such as $GABA_B$ that are also known to be important for the generation of cortical oscillations in microcircuits.[53–55]

## RESOURCE AVAILABILITY

### Lead contact

Requests for further information and resources should be directed to and will be fulfilled by the lead contact, Satu Palva (satu.palva@helsinki.fi).

### Materials availability

Ethical restrictions apply to data and original neuroimaging time series cannot be shared on a public server. Original PS and AC data underlying figures, statistics, and main conclusions have been uploaded to Dryad server.

### Data and code availability

- **Data**: We utilized the neurotransmitter receptor and transporter maps by Hansen et al.[31] which is freely accessible online (link in key resources table). Original PS and AC data and metadata have been deposited with Dryad. The DOI can be found in the key resources table.
- **Code**: We used the freely available Freesurfer and MNE-python software for preprocessing. All analyses were carried out in python, using freely available standard packages as well as custom code which we have shared on Github. Links are provided in the key resources table.
- **Additional information**: Any additional information required to reanalyze the data reported in this paper is available from the lead contact upon request.

## ACKNOWLEDGMENTS

We thank Victoria Puig for helpful discussion and comments on an earlier version of this manuscript.

This work was supported by the Academy of Finland with grants 1266745 and 1296304 to J.M.P. and 325404 to S.P. and by the Cultural Foundation of Finland with grants 00220945 and 00242647 to F.S.

## AUTHOR CONTRIBUTIONS

F.S., S.P., and J.M.P. conceptualized the study, F.S. carried out data acquisition and all analyses. All authors wrote the manuscript.

## DECLARATION OF INTERESTS

The authors declare no competing interests.

## STAR★METHODS

Detailed methods are provided in the online version of this paper and include the following:

- KEY RESOURCES TABLE
- EXPERIMENTAL MODEL AND STUDY PARTICIPANT DETAILS
  - Human participants
  - Neuroimaging data
  - Informed consent
- METHOD DETAILS
  - Neurotransmitter receptor and transporter maps and principal components
  - MEG data preprocessing and filtering
- QUANTIFICATION AND STATISTICAL ANALYSIS
  - Analysis of inter-areal phase synchrony and amplitude correlations
  - Covariance of receptor and transporter densities with node centrality

## SUPPLEMENTAL INFORMATION

Supplemental information can be found online at https://doi.org/10.1016/j.isci.2024.111111.

Received: February 22, 2024
Revised: July 6, 2024
Accepted: October 2, 2024
Published: October 9, 2024

## REFERENCES

1. Pesaran, B., Vinck, M., Einevoll, G.T., Sirota, A., Fries, P., Siegel, M., Truccolo, W., Schroeder, C.E., and Srinivasan, R. (2018). Investigating large-scale brain dynamics using field potential recordings: analysis and interpretation. Nat. Neurosci. *21*, 903–919. https://doi.org/10.1038/s41593-018-0171-8.
2. Palva, S., and Palva, J.M. (2012). Discovering Oscillatory Interaction Networks with M/EEG: Challenges and Breakthroughs. Trends Cognit. Sci. *16*, 219–230. https://doi.org/10.1016/j.tics.2012.02.004.
3. Deco, G., Buehlmann, A., Masquelier, T., and Hugues, E. (2011). The Role of Rhythmic Neural Synchronization in Rest and Task Conditions. Front. Hum. Neurosci. *5*, 4. https://doi.org/10.3389/fnhum.2011.00004.
4. Siegel, M., Donner, T.H., and Engel, A.K. (2012). Spectral fingerprints of large-scale neuronal interactions. Nat. Rev. Neurosci. *13*, 121–134. https://doi.org/10.1038/nrn3137.
5. Fries, P. (2015). Rhythms for Cognition: Communication through Coherence. Neuron *88*, 220–235. https://doi.org/10.1016/j.neuron.2015.09.034.
6. Singer, W. (1999). Neuronal Synchrony: A Versatile Code Review for the Definition of Relations? Neuron *24*, 49–65.
7. Sauseng, P., and Klimesch, W. (2008). What does phase information of oscillatory brain activity tell us about cognitive processes? Neurosci. Biobehav. Rev. *32*, 1001–1013. https://doi.org/10.1016/j.neubiorev.2008.03.014.
8. Vinck, M., Uran, C., Spyropoulos, G., Onorato, I., Broggini, A.C., Schneider, M., and Canales-Johnson, A. (2023). Principles of large-scale neural interactions. Neuron *111*, 987–1002. https://doi.org/10.1016/j.neuron.2023.03.015.
9. Womelsdorf, T., Schoffelen, J.-M., Oostenveld, R., Singer, W., Desimone, R., Engel, A.K., and Fries, P. (2007). Modulation of Neuronal Interactions Through Neuronal Synchronization. Science *316*, 1609–1612. https://doi.org/10.1126/science.1139597.
10. Engel, A.K., Fries, P., and Singer, W. (2001). Dynamic Predictions: Oscillations and synchrony in top-down processing. Nat. Rev. Neurosci. *2*, 704–716. https://doi.org/10.1038/35094565.
11. Avena-Koenigsberger, A., Misic, B., and Sporns, O. (2017). Communication dynamics in complex brain networks. Nat. Rev. Neurosci. *19*, 17–33. https://doi.org/10.1038/nrn.2017.149.
12. Lobier, M., Palva, J.M., and Palva, S. (2018). High-alpha band synchronization across frontal, parietal and visual cortex mediates behavioral and neuronal effects of visuospatial attention. Neuroimage *165*, 222–237. https://doi.org/10.1016/j.neuroimage.2017.10.044.
13. Hirvonen, J., Monto, S., Wang, S.H., Palva, J.M., and Palva, S. (2018). Dynamic large-scale network synchronization from perception to action. Netw. Neurosci. *2*, 442–463. https://doi.org/10.1162/netn_a_00039.
14. Rouhinen, S., Siebenhühner, F., Palva, J.M., and Palva, S. (2020). Spectral and anatomical patterns of large-scale synchronization predict human attentional capacity. Cerebr. Cortex *30*, 5293–5308. https://doi.org/10.1093/cercor/bhaa110.
15. Siebenhühner, F., Wang, S.H., Arnulfo, G., Lampinen, A., Nobili, L., Palva, J.M., and Palva, S. (2020). Genuine cross-frequency coupling networks in human resting-state electrophysiological recordings. PLoS Biol. *18*. https://doi.org/10.1371/journal.pbio.3000685.
16. de Pasquale, F., Spadone, S., Betti, V., Corbetta, M., and Della Penna, S. (2021). Temporal modes of hub synchronization at rest. Neuroimage *235*, 118005. https://doi.org/10.1016/j.neuroimage.2021.118005.
17. Traub, R.D., Bibbig, A., LeBeau, F.E.N., Buhl, E.H., and Whittington, M.A. (2004). Cellular Mechanisms of neuronal population oscillations in the hippocampus *in vitro*. Annu. Rev. Neurosci. *27*, 247–278. https://doi.org/10.1146/annurev.neuro.27.070203.144303.
18. Voloh, B., and Womelsdorf, T. (2016). A Role of Phase-Resetting in Coordinating Large Scale Neural Networks During Attention and Goal-Directed Behavior. Front. Syst. Neurosci. *10*, 18. https://doi.org/10.3389/fnsys.2016.00018.
19. Onslow, A.C.E., Jones, M.W., and Bogacz, R. (2014). A Canonical Circuit for Generating Phase-Amplitude Coupling. PLoS One *9*, e102591. https://doi.org/10.1371/journal.pone.0102591.
20. Buzśaki, G., and Wang, X.J. (2012). Mechanisms of gamma oscillations. Annu. Rev. Neurosci. *35*, 203–225. https://doi.org/10.1146/annurev-neuro-062111-150444.
21. Roopun, A.K., Kramer, M.A., Carracedo, L.M., Kaiser, M., Davies, C.H., Traub, R.D., Kopell, N.J., and Whittington, M.A. (2008). Temporal interactions between cortical rhythms. Front. Neurosci. *2*, 145–154. https://doi.org/10.3389/neuro.01.034.2008.

22. Batista-Brito, R., Zagha, E., Ratliff, J.M., and Vinck, M. (2018). Modulation of cortical circuits by top-down processing and arousal state in health and disease. Curr. Opin. Neurobiol. *52*, 172–181. https://doi.org/10.1016/j.conb.2018.06.008.
23. Buzsáki, G., Kaila, K., and Raichle, M. (2007). Inhibition and Brain Work. Neuron *56*, 771–783. https://doi.org/10.1016/j.neuron.2007.11.008.
24. Shine, J.M., Müller, E.J., Munn, B., Cabral, J., Moran, R.J., and Breakspear, M. (2021). Computational models link cellular mechanisms of neuromodulation to large-scale neural dynamics. Nat. Neurosci. *24*, 765–776. https://doi.org/10.1038/s41593-021-00824-6.
25. Cannon, J., McCarthy, M.M., Lee, S., Lee, J., Börgers, C., Whittington, M.A., and Kopell, N. (2014). Neurosystems: brain rhythms and cognitive processing. Eur. J. Neurosci. *39*, 705–719. https://doi.org/10.1111/ejn.12453.
26. Koh, W., Kwak, H., Cheong, E., and Lee, C.J. (2023). GABA tone regulation and its cognitive functions in the brain. Nat. Rev. Neurosci. *24*, 523–539. https://doi.org/10.1038/s41583-023-00724-7.
27. Villalobos, N. (2024). Disinhibition Is an Essential Network Motif Coordinated by GABA Levels and GABA B Receptors. Int. J. Mol. Sci. *25*, 1340. https://doi.org/10.3390/ijms25021340.
28. Sanchez-Vives, M.V., Barbero-Castillo, A., Perez-Zabalza, M., and Reig, R. (2021). GABAB receptors: modulation of thalamocortical dynamics and synaptic plasticity. Neuroscience *456*, 131–142. https://doi.org/10.1016/j.neuroscience.2020.03.011.
29. Avery, M.C., and Krichmar, J.L. (2017). Neuromodulatory Systems and Their Interactions: A Review of Models, Theories, and Experiments. Front. Neural Circ. *11*, 108. https://doi.org/10.3389/fncir.2017.00108.
30. Deco, G., and Kringelbach, M.L. (2017). Hierarchy of Information Processing in the Brain: A Novel 'Intrinsic Ignition' Framework. Neuron *94*, 961–968. https://doi.org/10.1016/j.neuron.2017.03.028.
31. Hansen, J.Y., Shafiei, G., Markello, R.D., Smart, K., Cox, S.M.L., Nørgaard, M., Beliveau, V., Wu, Y., Gallezot, J.-D., Aumont, É., et al. (2022). Mapping neurotransmitter systems to the structural and functional organization of the human neocortex. Nat. Neurosci. *25*, 1569–1581. https://doi.org/10.1038/s41593-022-01186-3.
32. Liu, Z.-Q., Shafiei, G., Baillet, S., and Misic, B. (2023). Spatially heterogeneous structure-function coupling in haemodynamic and electromagnetic brain networks. Neuroimage *278*, 120276. https://doi.org/10.1016/j.neuroimage.2023.120276.
33. Shafiei, G., Fulcher, B.D., Voytek, B., Satterthwaite, T.D., Baillet, S., and Misic, B. (2023). Neurophysiological signatures of cortical micro-architecture. Nat. Commun. *14*, 6000. https://doi.org/10.1038/s41467-023-41689-6.
34. Schaefer, A., Kong, R., Gordon, E.M., Laumann, T.O., Zuo, X.-N., Holmes, A.J., Eickhoff, S.B., and Yeo, B.T.T. (2018). Local-Global Parcellation of the Human Cerebral Cortex from Intrinsic Functional Connectivity MRI. Cerebr. Cortex *28*, 3095–3114. https://doi.org/10.1093/cercor/bhx179.
35. Markello, R.D., Hansen, J.Y., Liu, Z.-Q., Bazinet, V., Shafiei, G., Suárez, L.E., Blostein, N., Seidlitz, J., Baillet, S., Satterthwaite, T.D., et al. (2022). neuromaps: structural and functional interpretation of brain maps. Nat. Methods *19*, 1472–1479. https://doi.org/10.1038/s41592-022-01625-w.
36. Wiesman, A.I., da Silva Castanheira, J., Fon, E.A., and Baillet, S.; PREVENT-AD Research Group; Quebec Parkinson Network (2024). Alterations of Cortical Structure and Neurophysiology in Parkinson's Disease Are Aligned with Neurochemical Systems. Ann. Neurol. *95*, 802–816. https://doi.org/10.1002/ana.26871.
37. Hansen, J.Y., Shafiei, G., Vogel, J.W., Smart, K., Bearden, C.E., Hoogman, M., Franke, B., van Rooij, D., Buitelaar, J., McDonald, C.R., et al. (2022). Local molecular and global connectomic contributions to cross-disorder cortical abnormalities. Nat. Commun. *13*, 4682. https://doi.org/10.1038/s41467-022-32420-y.
38. Hansen, J.Y., Shafiei, G., Voigt, K., Liang, E.X., Cox, S.M.L., Leyton, M., Jamadar, S.D., and Misic, B. (2023). Integrating multimodal and multiscale connectivity blueprints of the human cerebral cortex in health and disease. PLoS Biol. *21*, e3002314. https://doi.org/10.1371/journal.pbio.3002314.
39. Weiss, E., Kann, M., and Wang, Q. (2023). Neuromodulation of Neural Oscillations in Health and Disease. Biology *12*, 371. https://doi.org/10.3390/biology12030371.
40. Luppi, A.I., Hansen, J.Y., Adapa, R., Carhart-Harris, R.L., Roseman, L., Timmermann, C., Golkowski, D., Ranft, A., Ilg, R., Jordan, D., et al. (2023). In vivo mapping of pharmacologically induced functional reorganization onto the human brain's neurotransmitter landscape. Sci. Adv. *9*, eadf8332. https://doi.org/10.1126/sciadv.adf8332.
41. Celada, P., Puig, M.V., and Artigas, F. (2013). Serotonin modulation of cortical neurons and networks. Front. Integr. Neurosci. *7*, 25. https://doi.org/10.3389/fnint.2013.00025.
42. Palva, J.M., Wang, S.H., Palva, S., Zhigalov, A., Monto, S., Brookes, M.J., Schoffelen, J.M., and Jerbi, K. (2018). Ghost interactions in MEG/EEG source space: A note of caution on inter-areal coupling measures. Neuroimage *173*, 632–643. https://doi.org/10.1016/j.neuroimage.2018.02.032.
43. Brookes, M.J., Woolrich, M.W., and Barnes, G.R. (2012). Measuring functional connectivity in MEG: A multivariate approach insensitive to linear source leakage. Neuroimage *63*, 910–920. https://doi.org/10.1016/j.neuroimage.2012.03.048.
44. Hipp, J.F., Hawellek, D.J., Corbetta, M., Siegel, M., and Engel, A.K. (2012). Large-scale cortical correlation structure of spontaneous oscillatory activity. Nat. Neurosci. *15*, 884–890. https://doi.org/10.1038/nn.3101.
45. Siems, M., and Siegel, M. (2020). Dissociated neuronal phase- and amplitude-coupling patterns in the human brain. Neuroimage *209*, 116538. https://doi.org/10.1016/j.neuroimage.2020.116538.
46. Simola, J., Siebenhühner, F., Myrov, V., Kantojärvi, K., Paunio, T., Palva, J.M., Brattico, E., and Palva, S. (2022). Genetic polymorphisms in COMT and BDNF influence synchronization dynamics of human neuronal oscillations. iScience *25*, 104985. https://doi.org/10.1016/j.isci.2022.104985.
47. Engel, A.K., Gerloff, C., Hilgetag, C.C., and Nolte, G. (2013). Intrinsic Coupling Modes: Multiscale Interactions in Ongoing Brain Activity. Neuron *80*, 867–886. https://doi.org/10.1016/j.neuron.2013.09.038.
48. Zhigalov, A., Arnulfo, G., Nobili, L., Palva, S., and Palva, J.M. (2017). Modular co-organization of functional connectivity and scale-free dynamics in the human brain. Netw. Neurosci. *1*, 143–165. https://doi.org/10.1162/netn_a_00008.
49. Sporns, O., Honey, C.J., and Kötter, R. (2007). Identification and Classification of Hubs in Brain Networks. PLoS One *2*, e1049. https://doi.org/10.1371/journal.pone.0001049.
50. Bullmore, E., and Sporns, O. (2009). Complex brain networks: graph theoretical analysis of structural and functional systems. Nat. Rev. Neurosci. *10*, 186–198. https://doi.org/10.1038/nrn2575.
51. Markello, R.D., and Misic, B. (2021). Comparing spatial null models for brain maps. Neuroimage *236*, 118052. https://doi.org/10.1016/j.neuroimage.2021.118052.
52. Middleton, S., Jalics, J., Kispersky, T., LeBeau, F.E.N., Roopun, A.K., Kopell, N.J., Whittington, M.A., and Cunningham, M.O. (2008). NMDA receptor-dependent switching between different gamma rhythm-generating microcircuits in entorhinal cortex. Proc. Natl. Acad. Sci. USA *105*, 18572–18577. https://doi.org/10.1073/pnas.0809302105.
53. Lozano-Soldevilla, D., ter Huurne, N., Cools, R., and Jensen, O. (2014). GABAergic Modulation of Visual Gamma and Alpha Oscillations and Its Consequences for Working Memory Performance. Curr. Biol. *24*, 2878–2887. https://doi.org/10.1016/j.cub.2014.10.017.
54. Lu, Z., Wang, H., Gu, J., and Gao, F. (2022). Association between abnormal brain oscillations and cognitive performance in patients with bipolar disorder: Molecular mechanisms and clinical evidence. Synapse *76*, e22247. https://doi.org/10.1002/syn.22247.
55. Liley, D.T.J., and Muthukumaraswamy, S.D. (2020). Evidence that alpha blocking is due to increases in system-level oscillatory damping not neuronal population desynchronisation. Neuroimage *208*, 116408. https://doi.org/10.1016/j.neuroimage.2019.116408.
56. Siebenhühner, F., Wang, S.H., Palva, J.M., and Palva, S. (2016). Cross-frequency synchronization connects networks of fast and slow oscillations during visual working memory maintenance. Elife *5*, e13451. https://doi.org/10.7554/eLife.13451.001.
57. Singer, W. (2013). Cortical dynamics revisited. Trends Cognit. Sci. *17*, 616–626. https://doi.org/10.1016/j.tics.2013.09.006.
58. Cabral, J., Kringelbach, M.L., and Deco, G. (2014). Exploring the Network Dynamics Underlying Brain Activity during Rest. Prog. Neurobiol. *114*, 102–131. https://doi.org/10.1016/j.pneurobio.2013.12.005.
59. Hipp, J.F., and Siegel, M. (2015). BOLD fMRI Correlation Reflects Frequency-Specific Neuronal Correlation. Curr. Biol. *25*, 1368–1374. https://doi.org/10.1016/j.cub.2015.03.049.
60. D'Andrea, A., Chella, F., Marshall, T.R., Pizzella, V., Romani, G.L., Jensen, O., and Marzetti, L. (2019). Alpha and alpha-beta phase synchronization mediate the recruitment of the visuospatial attention network through the Superior Longitudinal Fasciculus. Neuroimage *188*, 722–732. https://doi.org/10.1016/j.neuroimage.2018.12.056.
61. Klimesch, W. (2012). Alpha-band oscillations, attention, and controlled access to stored information. Trends Cognit. Sci. *16*, 606–617. https://doi.org/10.1016/j.tics.2012.10.007.

62. Klimesch, W., Sauseng, P., and Hanslmayr, S. (2007). EEG alpha oscillations: The inhibition-timing hypothesis. Brain Res. Rev. *53*, 63–88. https://doi.org/10.1016/j.brainresrev.2006.06.003.
63. Palva, S., and Palva, J.M. (2007). New vistas for α-frequency band oscillations. Trends Neurosci. *30*, 150–158. https://doi.org/10.1016/j.tins.2007.02.001.
64. Shaw, A.D., Chandler, H.L., Hamandi, K., Muthukumaraswamy, S.D., Hammers, A., and Singh, K.D. (2021). Tiagabine induced modulation of oscillatory connectivity and activity match PET-derived, canonical GABA-A receptor distributions. Eur. Neuropsychopharmacol. *50*, 34–45. https://doi.org/10.1016/j.euroneuro.2021.04.005.
65. Kopell, N.J., Gritton, H.J., Whittington, M.A., and Kramer, M.A. (2014). Beyond the Connectome: The Dynome. Neuron *83*, 1319–1328. https://doi.org/10.1016/j.neuron.2014.08.016.
66. Honey, C.J., Sporns, O., Cammoun, L., Gigandet, X., Thiran, J.P., Meuli, R., and Hagmann, P. (2009). Predicting human resting-state functional connectivity from structural connectivity. Proc. Natl. Acad. Sci. USA *106*, 2035–2040. https://doi.org/10.1073/pnas.0811168106.
67. Preti, M.G., and Van De Ville, D. (2019). Decoupling of brain function from structure reveals regional behavioral specialization in humans. Nat. Commun. *10*, 4747. https://doi.org/10.1038/s41467-019-12765-7.
68. Williams, N., Ojanperä, A., Siebenhühner, F., Toselli, B., Palva, S., Arnulfo, G., Kaski, S., and Palva, J.M. (2023). The influence of inter-regional delays in generating large-scale brain networks of phase synchronization. Neuroimage *279*, 120318. https://doi.org/10.1016/j.neuroimage.2023.120318.
69. Fuscà, M., Siebenhühner, F., Wang, S.H., Myrov, V., Arnulfo, G., Nobili, L., Palva, J.M., and Palva, S. (2023). Brain criticality predicts individual levels of inter-areal synchronization in human electrophysiological data. Nat. Commun. *14*, 4736. https://doi.org/10.1038/s41467-023-40056-9.
70. Pfeffer, T., Avramiea, A.E., Nolte, G., Engel, A.K., Linkenkaer-Hansen, K., and Donner, T.H. (2018). Catecholamines alter the intrinsic variability of cortical population activity and perception. PLoS Biol. *16*, e2003453. https://doi.org/10.1371/journal.pbio.2003453.
71. Shine, J.M. (2023). Neuromodulatory control of complex adaptive dynamics in the brain. Interface Focus *13*, 20220079. https://doi.org/10.1098/rsfs.2022.0079.
72. Başar, E., and Güntekin, B. (2008). A review of brain oscillations in cognitive disorders and the role of neurotransmitters. Brain Res. *1235*, 172–193. https://doi.org/10.1016/j.brainres.2008.06.103.
73. Koch, M., Schmiedt-Fehr, C., and Mathes, B. (2016). Neuropharmacology of altered brain oscillations in schizophrenia. Int. J. Psychophysiol. *103*, 62–68. https://doi.org/10.1016/j.ijpsycho.2015.02.014.
74. Nutt, D.J. (2008). Relationship of neurotransmitters to the symptoms of major depressive disorder. J. Clin. Psychiatry *69*, 4–7.
75. Celada, P., Puig, M., Amargós-Bosch, M., Adell, A., and Artigas, F. (2004). The therapeutic role of 5-HT1A and 5-HT2A receptors in depression. J. Psychiatry Neurosci. *29*, 252–265.
76. Fitzgerald, P.J., and Watson, B.O. (2018). Gamma oscillations as a biomarker for major depression: an emerging topic. Transl. Psychiatry *8*, 177. https://doi.org/10.1038/s41398-018-0239-y.
77. Tellioglu, T., and Robertson, D. (2001). Genetic or acquired deficits in the norepinephrine transporter: current understanding of clinical implications. Expert Rev. Mol. Med. *2001*, 1–10. https://doi.org/10.1017/S1462399401003878.
78. Volkow, N.D., Wang, G.-J., Kollins, S.H., Wigal, T.L., Newcorn, J.H., Telang, F., Fowler, J.S., Zhu, W., Logan, J., Ma, Y., et al. (2009). Evaluating Dopamine Reward Pathway in ADHD. JAMA *302*, 1084–1091. https://doi.org/10.1001/jama.2009.1308.
79. Banerjee, E., and Nandagopal, K. (2015). Does serotonin deficit mediate susceptibility to ADHD? Neurochem. Int. *82*, 52–68. https://doi.org/10.1016/j.neuint.2015.02.001.
80. Edden, R.A.E., Crocetti, D., Zhu, H., Gilbert, D.L., and Mostofsky, S.H. (2012). Reduced GABA Concentration in Attention-Deficit/Hyperactivity Disorder. Arch. Gen. Psychiatry *69*, 750–753. https://doi.org/10.1001/archgenpsychiatry.2011.2280.
81. Ibanez, A., Kringelbach, M.L., and Deco, G. (2024). A synergetic turn in cognitive neuroscience of brain diseases. Trends Cognit. Sci. *28*, 319–338. https://doi.org/10.1016/j.tics.2023.12.006.
82. Amunts, K., Mohlberg, H., Bludau, S., and Zilles, K. (2020). Julich-Brain: A 3D probabilistic atlas of the human brain's cytoarchitecture. Science *369*, 988–992. https://doi.org/10.1126/science.abb4588.
83. Honey, C.J., Thivierge, J.-P., and Sporns, O. (2010). Can structure predict function in the human brain? Neuroimage *52*, 766–776. https://doi.org/10.1016/j.neuroimage.2010.01.071.
84. Pang, J.C., Aquino, K.M., Oldehinkel, M., Robinson, P.A., Fulcher, B.D., Breakspear, M., and Fornito, A. (2023). Geometric constraints on human brain function. Nature *618*, 566–574. https://doi.org/10.1038/s41586-023-06098-1.
85. Arnulfo, G., Hirvonen, J., Nobili, L., Palva, S., and Palva, J.M. (2015). Phase and amplitude correlations in resting-state activity in human stereotactical EEG recordings. Neuroimage *112*, 114–127. https://doi.org/10.1016/j.neuroimage.2015.02.031.
86. Arnulfo, G., Wang, S.H., Myrov, V., Toselli, B., Hirvonen, J., Fato, M.M., Nobili, L., Cardinale, F., Rubino, A., Zhigalov, A., et al. (2020). Long-range phase synchronization of high-frequency oscillations in human cortex. Nat. Commun. *11*, 5363. https://doi.org/10.1038/s41467-020-18975-8.
87. Boot, N., Baas, M., van Gaal, S., Cools, R., and De Dreu, C.K.W. (2017). Creative cognition and dopaminergic modulation of fronto-striatal networks: Integrative review and research agenda. Neurosci. Biobehav. Rev. *78*, 13–23. https://doi.org/10.1016/j.neubiorev.2017.04.007.
88. Cools, R. (2008). Role of Dopamine in the Motivational and Cognitive Control of Behavior. Neuroscientist *14*, 381–395. https://doi.org/10.1177/1073858408317009.
89. Puig, M.V., and Gulledge, A.T. (2011). Serotonin and Prefrontal Cortex Function: Neurons, Networks, and Circuits. Mol. Neurobiol. *44*, 449–464. https://doi.org/10.1007/s12035-011-8214-0.
90. Gramfort, A., Luessi, M., Larson, E., Engemann, D.A., Strohmeier, D., Brodbeck, C., Parkkonen, L., and Hämäläinen, M.S. (2014). MNE software for processing MEG and EEG data. Neuroimage *86*, 446–460. https://doi.org/10.1016/j.neuroimage.2013.10.027.
91. Blondel, V.D., Guillaume, J.-L., Lambiotte, R., and Lefebvre, E. (2008). Fast unfolding of communities in large networks. J. Stat. Mech. *2008*, P10008.
92. Alexander-Bloch, A.F., Shou, H., Liu, S., Satterthwaite, T.D., Glahn, D.C., Shinohara, R.T., Vandekar, S.N., and Raznahan, A. (2018). On testing for spatial correspondence between maps of human brain structure and function. Neuroimage *178*, 540–551. https://doi.org/10.1016/j.neuroimage.2018.05.070.
93. Bazinet, V., Hansen, J.Y., and Misic, B. (2023). Towards a biologically annotated brain connectome. Nat. Rev. Neurosci. *24*, 747–760. https://doi.org/10.1038/s41583-023-00752-3.

# STAR★METHODS

## KEY RESOURCES TABLE

| REAGENT or RESOURCE | SOURCE | IDENTIFIER |
|---|---|---|
| Deposited data | | |
| Neurotransmitter receptor and transporter density maps | Hansen et al.[31] | https://github.com/netneurolab/hansen_receptors |
| MEG phase synchrony and amplitude correlation data | This paper | Dryad data: https://doi.org/10.5061/dryad.qz612jmq1 |
| Software and algorithms | | |
| Freesurfer | Open Source | http://surfer.nmr.mgh.harvard.edu/ |
| MNE | Open Source | https://mne.tools/stable/index.html |
| Python | Python Software Foundation | https://www.python.org/ |
| Python code used in this paper | Original code | https://github.com/palvalab/receptor_centrality |

## EXPERIMENTAL MODEL AND STUDY PARTICIPANT DETAILS

### Human participants

Data from 67 healthy human volunteers (age 18 to 57 years old; mean age: 30.9 ± 8.3 years; 6 left-handed; 32 female, 35 male; 65 Caucasian, 2 East Asian) were collected for this study. Demographics are provided in Table S1. This sample size is sufficient to detect correlations of at least r = 0.34 at an $\alpha$-level of 0.05 with statistical power of 80%.

### Neuroimaging data

MEG data was recorded with a 306-channel (204 planar gradiometers and 102 magnetometers) Triux MEG (Elekta-Neuromag/MEGIN, Helsinki, Finland) at the BioMag Laboratory, HUS Medical Imaging Center. We recorded 10 minutes of eyes-open resting-state data from all participants. Bipolar horizontal and vertical EOG were recorded for the detection of ocular artifacts. MEG and EOG were recorded at a 1,000-Hz sampling rate.

T1-weighted anatomical MRI scans (MP-RAGE) were obtained for head models and cortical surface reconstruction at a resolution of 1 × 1 × 1 mm with a 1.5-Tesla MRI scanner (Siemens, Munich, Germany) at Helsinki University Central Hospital.

### Informed consent

All participants gave a written informed consent prior to the recordings. The study protocol for MEG and MRI data obtained in the University of Helsinki was approved by the Coordinating Ethical Committee of Helsinki University Central Hospital (HUCH) (ID 290/13/03/2013). The study was performed in accordance with the Declaration of Helsinki.

## METHOD DETAILS

### Neurotransmitter receptor and transporter maps and principal components

We downloaded the code and dataset from https://github.com/netneurolab/hansen_receptors and computed the receptor density in each of the 200 parcels for 35 different receptor and transporter maps. This dataset has been recently described in detail earlier.[31] Where several maps were available for the same receptor or transporter, we computed the mean value, with each map weighted by the number of subjects, thus obtaining 19 density maps (*see* Figure S1). We used the PCA algorithm from the python toolkit *scikit-learn* to identify the first 5 principal components (PCs) underlying the receptor and transporter maps (*see* Figure 1 *and* results: principal component analysis reveals neuroarchitectonical principles underlying density maps of neurotransmitter receptors and transporters).

### MEG data preprocessing and filtering

Volumetric segmentation of MRI data, flattening, cortical parcellation, and neuroanatomical labeling were carried out for each of the 67 subjects individually using FreeSurfer software (http://surfer.nmr.mgh.harvard.edu). We used the Schaefer atlas with 200 parcels.[34] MNE software[90] (https://mne.tools/stable/index.html) was used for the preparation of cortically constrained source models for MEG–MRI colocalization, forward and inverse operators. The source models had dipole orientations fixed to pial-surface normals and a 5-mm inter-dipole separation throughout the cortex, where hemispheres had between 5080–7645 active source vertices.

Temporal signal space separation (tSSS) in the Maxfilter software (Elekta-Neuromag) was used to suppress extracranial noise from MEG sensors and to interpolate bad channels. We used independent components analysis (ICA) adapted from the MATLAB toolbox Fieldtrip (http://www.fieldtriptoolbox.org) to extract and identify components that were correlated with ocular artifacts (identified using the EOG signal), heartbeat artifacts (identified using the magnetometer signal as a reference), or muscle artifacts. We estimated vertex fidelity by

applying forward and inverse operators to complex white-noise time series and computing the correlation between original and forward-inverse-modeled time series. Using these fidelity estimates, we obtained fidelity-weighted inverse operators that were used for the inverse modeling of the real data with high reconstruction accuracy.[15] After source reconstruction, the time-series data were collapsed to the 200 cortical parcels and then filtered into narrowband time series using a bank of 41 Morlet filters with wavelet width parameter m = 5 and approximately log-linear spacing of center frequencies ranging from 1.1 to 95.6 Hz (*see* Figure 2A).

## QUANTIFICATION AND STATISTICAL ANALYSIS

All quantification and statistical analysis were carried out in custom python code.

### Analysis of inter-areal phase synchrony and amplitude correlations

To estimate pairwise phase synchrony between parcels, we estimated the complex phase-locking value (cPLV):

$$cPLV_{a,b} = \frac{1}{N}\sum_{n} exp\{i(\theta_a - \theta_b)\}$$

where $\theta_a$ and $\theta_b$ are the instantaneous phase time series of the complex analytical narrowband time series $X_a$ and $X_b$, and $N$ is the number of samples $n$.

From the cPLV, the "classical" PLV can be derived as $PLV = |cPLV|$ and the imaginary PLV as $iPLV = |im(cPLV)|$. The imaginary PLV is insensitive to zero-lag false-positive interactions which are often spurious due to residual linear mixing after inverse modeling[42] and was therefore used in this study. Amplitude correlations were computed between the amplitude envelopes of the narrowband time series $X_a$ and $X_b$ with the orthogonalized correlation coefficient (oCC), where the time series $X_b$ is orthogonalized with respect to $X_a$ which also has the effect of eliminating spurious connections.[43,44] The grand average for each Morlet frequency was computed as the mean over all parcels and subjects (*see* Figure 2C) and the correlation between AC and PS in each frequency was estimated with Spearman's correlation coefficient.

For each frequency, we computed for each parcel the node strength, i.e., the mean connectivity strength of this parcel with all others (averaged over all 67 subjects). We computed the spatial similarity of node strength matrices between frequencies and then used the Louvain algorithm[91] to identify frequency clusters for both iPLV and oCC separately and then derived from these consensus ranges for 6 frequency bands (see Figure S2). We then obtained connectivity networks for each frequency band by averaging the networks of all individual frequencies within the band (*see* Figure S3). We then computed node strength for these networks as well, and further computed node degree and betweenness centrality (using the python toolkit *networkx*) in connectivity networks thresholded at edge densities 20% and 50%.[49,50]

### Covariance of receptor and transporter densities with node centrality

We then estimated, for each individual frequency as well as for all 6 frequency bands, the covariance of node centrality (indexed by node strength, node degree, or betweenness centrality) with receptor or transporter density, or with principal component maps, across all 200 parcels using Spearman's correlation coefficient (*see* Figures 2E–2J, 3, and S4–S7). In order to assess statistical significance, we performed N=10,000 permutations in which the parcel values in MEG data were shuffled within each hemisphere and estimated the $p_{perm}$ values from the comparison of $r_{real}$ against the distribution of $r_{perm}$. In order to correct for multiple comparisons, we discarded as many significant observations as could be expected to be false positives at the chosen $\alpha$ level of 0.05[15,46] (equaling 6 out of 19×6=114 observations for frequency bands and individual receptors, 2 out of 5×6=30 observations for frequency bands and PCs, and 39 out of 19×41=779 observations for Morlet frequencies and individual receptors), retaining the significant observations with the lowest p-values.

We also performed an additional, more conservative, 'spin' permutation test in which parcels, again within each hemisphere, are rotated randomly across the spherical surface in the freesurfer fsaverage surface. This method preserves in the permutated data spatial autocorrelations which are present in neuroimaging data and have been claimed to be a possible cause for false positives.[51,92,93] Adapting the procedure described in Hansen et al.[31], we again performed N=10,000 permutations and afterwards adjusted $p_{spin}$ values to account for the expected fraction of false positives as with the fully random approach.